



**QUEEN'S  
UNIVERSITY  
BELFAST**

## **Silicon Photoanodes for Solar-Driven Oxidation of Brine: A Nanoscale, Photo-Active Analog of the Dimensionally-Stable Anode**

O'Rourke, C., Tang Kong, R., Mills, A., & McIntyre, P. C. (2018). Silicon Photoanodes for Solar-Driven Oxidation of Brine: A Nanoscale, Photo-Active Analog of the Dimensionally-Stable Anode. *Journal of the Electrochemical Society*, 165(16), H1072-H1079. <https://doi.org/10.1149/2.0791816jes>

### **Published in:**

Journal of the Electrochemical Society

### **Document Version:**

Peer reviewed version

### **Queen's University Belfast - Research Portal:**

[Link to publication record in Queen's University Belfast Research Portal](#)

### **Publisher rights**

Copyright 2018 Electrochemical Society. This work is made available online in accordance with the publisher's policies. Please refer to any applicable terms of use of the publisher.

### **General rights**

Copyright for the publications made accessible via the Queen's University Belfast Research Portal is retained by the author(s) and / or other copyright owners and it is a condition of accessing these publications that users recognise and abide by the legal requirements associated with these rights.

### **Take down policy**

The Research Portal is Queen's institutional repository that provides access to Queen's research output. Every effort has been made to ensure that content in the Research Portal does not infringe any person's rights, or applicable UK laws. If you discover content in the Research Portal that you believe breaches copyright or violates any law, please contact [openaccess@qub.ac.uk](mailto:openaccess@qub.ac.uk).

### **Open Access**

This research has been made openly available by Queen's academics and its Open Research team. We would love to hear how access to this research benefits you. – Share your feedback with us: <http://go.qub.ac.uk/oa-feedback>

1 **Silicon Photoanodes for Solar-Driven Oxidation**  
2 **of Brine: A Nanoscale, Photo-Active Analog of**  
3 **the Dimensionally-Stable Anode**

4 Robert Tang-Kong<sup>a,†</sup>, Christopher O'Rourke<sup>b,†</sup>, Andrew Mills<sup>b</sup>, and Paul C. McIntyre<sup>a\*</sup>

5 a: Department of Materials Science & Engineering, Stanford University, California 94305, USA

6 b: Department of Chemistry and Chemical Engineering, Queens University Belfast, Stranmillis Road,  
7 Belfast, BT9 5AG, UK

8 † These authors contributed equally to this work

9 \* e-mail: [pcml@stanford.edu](mailto:pcml@stanford.edu)

10

11 **Abstract**

12 We report the first results in which ALD-TiO<sub>2</sub> layers electronically couple silicon to an overlying  
13 catalyst coating while inhibiting corrosion during brine splitting, a reaction that is capable of  
14 generating not only a fuel (H<sub>2</sub>) but also a disinfectant (Cl<sub>2</sub> or NaOCl). An n-type silicon photoanode,  
15 and a p<sup>+</sup>-silicon anode are protected by a 1.7 nm coating of amorphous TiO<sub>2</sub> and 2 nm coating of Ir.  
16 The p<sup>+</sup>-Si/TiO<sub>2</sub>/Ir anode is able to effect the oxidation of chloride (0.5 M H<sub>2</sub>SO<sub>4</sub>, 3.5 M NaCl) in the  
17 dark with a low overpotential compared to that for oxidation of water (0.5 M H<sub>2</sub>SO<sub>4</sub>). The 0.294 V  
18 overpotential difference occurs despite the difference in standard redox potentials,  $\Delta E = (E^\circ(\text{Cl}_2/\text{Cl}^-) -$   
19  $E^\circ(\text{O}_2/\text{H}_2\text{O}))$ , is 130 mV. Under 1 sun irradiation a photovoltage of *ca.* 0.566 V is achieved by  
20 comparing the illuminated n-Si/TiO<sub>2</sub>/Ir photoanode with the dark p<sup>+</sup>-silicon anode. Although the n-  
21 Si/TiO<sub>2</sub>/Ir photoanode is only one half of an eventual tandem cell needed for photosynthetic brine  
22 splitting, its ABPE for chloride oxidation is 1.42%, *ca.* 28 times that for water oxidation. The  
23 illuminated n-Si/TiO<sub>2</sub>/Ir photoanode remained stable at 1 mA cm<sup>-2</sup> during a six-day  
24 chronopotentiometry test.

25

26 **Key words:** silicon; anode; brine; chloride; oxidation; photoelectrochemistry

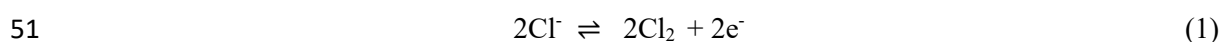
27

## 28 I. Introduction

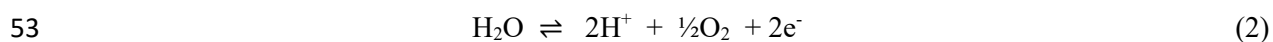
29 Conversion of solar to electrical energy using photovoltaic devices, such as the silicon solar cell is  
30 well-established, but solar energy is diurnal and intermittent and so there is least of it when we most  
31 need it, i.e. at night in winter. As a consequence, there is great interest in developing efficient,  
32 inexpensive and stable solar energy conversion devices that generate readily utilizable chemical  
33 fuels.<sup>1,2</sup> A popular, current approach is to develop a solar-driven, water-splitting system, since it uses  
34 the sun's energy to produce hydrogen, which can be stored, readily transported and used when  
35 needed.<sup>2</sup> However, the overpotential for water oxidation, using the best platinum group metal  
36 electrocatalysts<sup>1</sup>, is still typically 300-400 mV at 10 mA cm<sup>-2</sup> and so represents a major barrier to the  
37 creation of a long-lasting, high solar to chemical energy efficiency device.

38 Recently, Nocera et al. suggested that an inexpensive artificial leaf water splitting device will find  
39 initial and widespread application in the developing world at less urbanized, off-the-grid, locations.<sup>3,4</sup>  
40 Advantages of such photoelectrochemical cells (PEC's) which combine light absorption and catalyzed  
41 electrochemical reactions are 1) the potential simplicity of an integrated design, 2) their compact foot-  
42 print and 3) their ability to accommodate less expensive catalysts operating at electrolysis current  
43 densities better matched to solar photocurrent densities.

44 Compared to the photocleavage of water, the photo-electrolysis of brine has not been studied nearly as  
45 widely, despite the fact that the overpotential for chlorine production is low.<sup>5</sup> In addition, the  
46 electrolysis of salt water: (i) generates H<sub>2</sub>, alkali and Cl<sub>2</sub>, (or, H<sub>2</sub> and NaOCl, if the Cl<sub>2</sub> and caustic are  
47 allowed to combine), (ii) stores approximately the same amount of energy per electron as the water  
48 splitting reaction, and (iii) generates a more valuable chemical oxidant feedstock, namely, Cl<sub>2</sub> or  
49 NaOCl. However, it is not without its challenges, given the oxidation of chloride to chlorine in acid  
50 solution



52 has a significantly higher standard redox potential ( $E^\circ(\text{Cl}_2/\text{Cl}^-) = 1.36 \text{ V}$ ) than that of water



54 ( $E^\circ(\text{O}_2/\text{H}_2\text{O}) = 1.23 \text{ V}$ ). Moreover, chlorine is a very aggressive oxidant, with a solubility in water  
55 ( $0.092 \text{ mol dm}^{-3} \text{ atm}^{-1}$ ) that is over 70 x's that of  $\text{O}_2$ , thus increasing markedly the likelihood of its  
56 reaction with cell components, including, most importantly, the semiconductor photoanode.

57 The industrial production of  $\text{Cl}_2/\text{NaOCl}$  from brine is worth currently \$46 Bn in the USA alone.<sup>6</sup> Its  
58 role in disinfection is important, since the need for potable (i.e. disinfected) water worldwide is great,  
59 with a sixth of the world population (ca. 1.1 Bn people) having no access to improved water supplies  
60 and with a much greater number consuming contaminated water every day. It is estimated that >  
61 4000 children die of diarrhoea alone every day due to poor water quality.<sup>7</sup> There is, therefore, a  
62 compelling need for an inexpensive and compact solar-to-chemical energy conversion device capable  
63 of producing not only a fuel (hydrogen), for heating and for electricity (via a fuel cell), when the sun  
64 is not shining, but also a disinfectant – such as chlorine/hypochlorite – for use in generating potable  
65 water and clean surfaces.

66 Herein we report a silicon photoanode which functions both as a nanoscale version of the  
67 dimensionally-stable anode (DSA)<sup>8</sup>, the key technology in industrial chlor-alkali electrochemistry,  
68 and as an efficient absorber of solar light. This photoanode could function as a key junction in a  
69 multi-junction photoelectrochemical cell<sup>9</sup> for unassisted brine splitting. Industrial DSA electrodes  
70 have a high precious metal (Ir, Ru) loading and thick active layers<sup>10</sup> mixed with  $\text{TiO}_2$  and typically  
71 coating a Ti substrate.<sup>11,12</sup> However, such anodes typically operate at current densities that are 100 x's  
72 greater than those (ca.  $10 \text{ mA cm}^{-2}$ ) expected in any photosynthetic solar cell and In the reported  
73 nanoscale DSA structure, atomic layer deposited  $\text{TiO}_2$  is used to achieve stable brine splitting on  
74 silicon, which is otherwise unstable under the conditions used in chloride oxidation. The  $\text{TiO}_2$  thin  
75 film electronically couples an overlying chloride oxidation catalyst film, in the form of an ultra-thin  
76 iridium layer, to the silicon substrate, achieving a high yield for chlorine synthesis, photovoltages  
77 exceeding 560 mV and greater than 6 days of continuous operation during chronoamperometry  
78 testing.

## 79 **II. Experimental**

### 80 *Materials*

81 The silicon wafers used here were either: (i) heavily boron-doped p<sup>+</sup>-type Si (100) wafers ( $\rho = 0.001$ –  
82  $0.002 \text{ } \Omega \text{ cm}$ ,  $500 \text{ } \mu\text{m}$  thick), which were used as conductive silicon substrates to study water and  
83 chloride oxidation in the dark or (ii) lightly phosphorous-doped, n-type Si (100) wafers ( $\rho = 0.1$ – $0.2$   
84  $\Omega \text{ cm}$ ,  $500 \text{ } \mu\text{m}$  thick). The wafers were used as received, with a thin ( $< 2 \text{ nm}$ ) SiO<sub>2</sub> layer as prepared  
85 by the wafer supplier, Nova Electronic Materials. Onto both wafer types, a 1.7 nm amorphous TiO<sub>2</sub>  
86 layer was deposited via 30 cycles of atomic layer deposition, ALD, at 170°C with tetrakis-  
87 dimethylamido titanium, TDMAT, as the titanium source and H<sub>2</sub>O as the oxygen source. In all cases,  
88 this was followed by a coating of a 2 nm Ir layer, deposited by electron beam evaporation. The  
89 backside contacts for the n-Si and p<sup>+</sup>-Si substrates were e-beam evaporated Al and Pt, respectively.  
90 These two electrodes are referred to throughout as n-Si/TiO<sub>2</sub>/Ir and p<sup>+</sup>-Si/TiO<sub>2</sub>/Ir electrodes. A  
91 schematic of the n-Si/TiO<sub>2</sub>/Ir photoanode used in this work for the photoelectrolysis of acidified brine  
92 is illustrated in **Figure 1**.

93

#### 94 *Methods*

95 All electrochemical and photoelectrochemical experiments were conducted using  $0.5 \text{ mol dm}^{-3} \text{ H}_2\text{SO}_4$ ,  
96 in the absence (for water oxidation) and presence (for chloride oxidation) of  $3.5 \text{ mol dm}^{-3} \text{ NaCl}$ . All  
97 electrochemical work was performed using a modified version of the 'silo-like' electrochemical cell  
98 used by the McIntyre and Chidsey group,<sup>13</sup> which is illustrated in **Figure S1**. The cell components  
99 and design are described in the supporting information. The gas inlet and outlet of the cell were used  
100 in Cl<sub>2</sub> yield measurements to sweep out, using a continuous stream of Ar (flow rate:  $100 \text{ cm}^3 \text{ min}^{-1}$ ),  
101 the Cl<sub>2</sub> generated in the electrochemical cell into a  $100 \text{ cm}^3$  KI trap the spectrophotometric analysis of  
102 the latter allowed the total amount of Cl<sub>2</sub> to be assessed<sup>14</sup>. The bulk of the electrochemical  
103 measurements were conducted using a Metrohm Autolab (PGSTAT128N) potentiostat. All linear  
104 sweep voltammograms, LSVs, were recorded using a  $1 \text{ mV s}^{-1}$  sweep rate. Electrochemical  
105 impedance spectroscopy was performed using a FRA32M module (Metrohm) in order to determine  
106 the resistance of electrolytes used in this study and so compensate for the *i*R drop in the cell.

107 A sealed, quartz window recessed in the PTFE cap of the electrochemical cell allowed the flat, n-  
108 Si/TiO<sub>2</sub>/Ir anode, installed in the base of the cell, to be irradiated. Irradiations were conducted using  
109 either: (i) a high power 455 nm LED (HBW = 16 nm; OSLO<sup>+</sup> PowerStar Deep Blue 455 nm;  
110 maximum wattage > 2.2 W) providing an irradiance of ca. 6.5 mW cm<sup>-2</sup> (at ca. 7 cm above the  
111 electrode) for the chronopotentiometry experiments or, more usually, (ii) a 150 W solar simulator  
112 (Sciencetech SS150W) fitted with a AM1.5 filter, simulating the irradiance of 1 sun (ca. 100 mW cm<sup>-2</sup>,  
113 measured using a power meter, ThorLabs, PM100D). All UV/Vis spectra were recorded using an  
114 Agilent Cary 6000i UV/Vis/NIR spectrophotometer. IPCE measurements were made using a standard  
115 glass vial (A-001056, Biologic) with a PTFE cap holding all electrodes in place and a 1kW Xe-arc  
116 lamp (OBB KiloArc), coupled to a 200 mm meter Czerny-Turner monochromator (OBB), and Gooch  
117 & Housego (OL756) radiometer were used to provide the monochromatic light and associated  
118 irradiance values, respectively. IPCE measurements were conducted on a n-Si/TiO<sub>2</sub>/Ir photoanode  
119 (area: 0.8 cm<sup>2</sup>) polarised at 1.8 v vs NHE in an electrolyte volume of 15mL (0.5M H<sub>2</sub>SO<sub>4</sub> + 3.5 NaCl).

### 120 **III. Results and Discussion**

#### 121 *Optical measurements and initial photoelectrochemical studies*

122 Silicon, a candidate material for the low-gap semiconductor of a tandem device, has a band gap of 1.1  
123 eV and so absorbs strongly incident light of  $\lambda \leq 1127$  nm, as indicated by its reflectance spectrum  
124 which has been widely reported.<sup>15</sup>

125 In contrast to the absorption spectrum of Si, those of the protecting Ti oxide and the Ir film used in  
126 this work have not been reported previously. Thus, the UV/Vis/NIR absorption spectrum of the thin  
127 (1.7 nm) TiO<sub>2</sub> film, deposited using ALD on quartz, is illustrated in **Figure 2** and shows that it absorbs  
128 no visible light, i.e. it is colourless, and that it absorbs very little UV radiation. Thus, its presence will  
129 have very little effect on the amount of light absorbed by the underlying Si. In contrast, the  
130 absorption spectrum of the 2 nm Ir film, also illustrated in **Figure 2**, reveals an average absorbance of  
131 ca. 0.184 throughout the visible and NIR spectrum, which suggests that only ca. 65.5 % of the  
132 incident visible light is transmitted by the Ir film to the underlying Si. Thus, although the deposition

133 of an Ir film is convenient and relatively easy to effect, the use of the Ir catalyst in the form of a  
134 continuous film reduces the efficiency of the photoanode significantly by partly obscuring the surface  
135 of the Si. This implies that the photocurrent may be improved markedly if a pattern of catalyst islands  
136 is used instead of a film. This approach has been adopted in the work of Hu et al<sup>16</sup> who used 100 nm  
137 thick Ni-island electrocatalysts patterned in square arrays of 3  $\mu\text{m}$  diameter circles on a 7- $\mu\text{m}$  pitch, to  
138 cover thick (44 nm), but 'electronically leaky',  $\text{TiO}_2$  protective coatings on an n-Si photoanode film, so  
139 that the islands only blocked 14.4% of the electrode surface.

140 In order to quickly compare and contrast the efficacies of the n-Si/ $\text{TiO}_2$ /Ir photoanode for water  
141 oxidation (in 0.5 M  $\text{H}_2\text{SO}_4$ ) to that of chloride (in 0.5 M  $\text{H}_2\text{SO}_4$  plus 3.5 M NaCl), cyclic  
142 voltammograms photocurrents were recorded under 1 sun irradiation and the results of this work are  
143 illustrated in **Figure 4**.

144 Inspection of the results reveals that n-Si/ $\text{TiO}_2$ /Ir photoanode is able to effect the photo-oxidation of  
145 chloride to chlorine in acid at lower potentials (typically, ca. 300 mV lower at 1  $\text{mA cm}^{-2}$ ) than that  
146 for water oxidation, despite the fact that  $\Delta E = (E^\circ(\text{Cl}_2/\text{Cl}^-) - E^\circ(\text{O}_2/\text{H}_2\text{O})) = 130 \text{ mV}$ . This feature  
147 results from the much higher overpotential for water oxidation,  $\eta_{\text{O}_2}$ , ( $\eta_{\text{O}_2} \approx 0.428 \text{ V}$  on a p+-Si/ $\text{TiO}_2$ /Ir  
148 anode, vide infra) compared to that for chloride oxidation ( $\eta_{\text{Cl}_2} \approx \text{ca. } 0.134 \text{ V}$  on a p+-Si/ $\text{TiO}_2$ /Ir  
149 anode, vide infra).

150 In contrast, in 1 M NaOH, the primary chloride oxidation reaction is:



152 where,  $(E^\circ(\text{OCl}^-/\text{Cl}^-) = 0.81 \text{ V vs NHE}$ , so that  $\Delta E$ , now equal to:  $(E^\circ(\text{OCl}^-/\text{Cl}^-) - E^\circ(\text{O}_2/\text{OH}^-))$ , is much  
153 larger (406 mV), than the 130 mV in acid, and this mostly off-sets the benefit gained by having  $\eta_{\text{Cl}_2}$   
154  $\ll \eta_{\text{O}_2}$ . Thus, in 1 M NaOH the CV curves for water and chloride oxidation are no longer well  
155 separated, but overlap, so that the photoanode generates a mixture of hypochlorite and  $\text{O}_2$ . As a  
156 consequence, in order to simplify this study to that of either water or chloride oxidation, but not a  
157 mixture of both, the bulk of the work described here was carried out under acidic conditions (0.5 M  
158  $\text{H}_2\text{SO}_4$ ) with or without 3 M NaCl. In acidified brine the overall photo-electrochemical reaction is the



159 oxidation of chloride to  $\text{Cl}_2$ , i.e. reaction (1), at the n-Si/TiO<sub>2</sub>/Ir photoanode, and the concomitant  
160 reduction of  $\text{H}^+$  to  $\text{H}_2$  at the Pt counter electrode, as illustrated in **Figure 1**.

161 It can be shown<sup>13</sup> that solar irradiation at 1 sun provides ca.  $2.7 \times 10^{17}$  photons  $\text{cm}^{-2}$  with energies  $\geq$  the  
162 Si band gap, which in turn should produce a theoretical maximum photocurrent density of ca. 43 mA  
163  $\text{cm}^{-2}$ . From the results illustrated in **Figure 4**, the light-limited saturation currents for both water and  
164 chloride oxidation, achieved at high bias potentials, were found to be ca. 31 mA  $\text{cm}^{-2}$ , i.e. ca. 72% of  
165 the theoretical maximum. Given that ca. 35% of the incident light is obscured by the Ir film, the value  
166 of 72% implies that, at high bias potentials, the n-Si/TiO<sub>2</sub>/Ir photoanode, is ca. 100% efficient in  
167 converting photons to current, i.e. the photogenerated holes are readily and efficiently conducted  
168 through the TiO<sub>2</sub> overlayer to the Ir electrocatalyst. IPCE measurements were also made using the n-  
169 Si/TiO<sub>2</sub>/Ir photoanode biased at 1.8V vs NHE (Figure 4). The IPCE is high, across a wide range of  
170 wavelengths, and consistent with the average value of 72% reported above, suggesting that, once  
171 corrected for the absorbance due to the catalyst layers, this system, with its 1.8 V bias is ca. 100%  
172 efficient in converting photons to current.

173 The broken vertical lines in **Figure 4** represent the thermodynamic redox potentials for water (black)  
174 and chloride (red) oxidation in 0.5 M  $\text{H}_2\text{SO}_4$  and in both photo-electrochemical reactions, reasonable  
175 (up to 10 mA  $\text{cm}^{-2}$  and 1 mA  $\text{cm}^{-2}$  for  $\text{Cl}^-$  and  $\text{H}_2\text{O}$  oxidation, respectively) photocurrents are  
176 generated, by the n-Si/TiO<sub>2</sub>/Ir photoanode at 1 sun illumination, at potentials at and below these  
177 thermodynamic limits, suggesting a reasonable degree of solar to chemical energy conversion,  
178 although clearly much more so for chloride oxidation. However, as we shall see later, a useful  
179 assessment of the applied bias photon efficiency, ABPE, requires the cell to be operated in 2-  
180 electrode, rather than 3-electrode mode, and under such conditions the efficiency of cell is  
181 significantly reduced.

182 The above results show that, upon band gap illumination of the n-Si, the photogenerated holes in the  
183 Si valence band are able to move through the intermediate oxide layers, as illustrated in **Figure 1**, to  
184 the Ir layer, where they are then able to oxidize surface adsorbed water, or chloride, from the  
185 electrolyte solution. Further work on TiO<sub>2</sub>-protected Si anodes,<sup>19-22</sup> suggests that the unexpectedly

186 low barrier for hole conduction through the amorphous TiO<sub>2</sub> layer involves hole-tunnelling through an  
187 ultrathin (< 2 nm) SiO<sub>2</sub> interface layer and then a polaronic or hopping conduction mechanism  
188 through the TiO<sub>2</sub> protective layer to the Ir catalyst film. Importantly, in the absence of light, the  
189 current is negligible, i.e. < 1 μA cm<sup>-2</sup>, at the potentials used in **Figure 4**, due to the very low thermal  
190 population of holes in the n-Si. Thus, in the dark the n-Si/TiO<sub>2</sub>/Ir photoanode is not able to effect  
191 either the water oxidation or chloride oxidation half-cell reactions, but is able to do so upon  
192 illumination with ultra-band gap light, as illustrated by the photoelectrochemical data in **Figure 4**.

### 193 *LSV's: Tafel slopes, overpotentials and photovoltages*

194 Linear sweep voltammograms, LSVs, for water oxidation, i.e. reaction (2), were recorded for the n-  
195 Si/TiO<sub>2</sub>/Ir photoanode, under 1 sun illumination, and the p+-Si/TiO<sub>2</sub>/Ir anode (in the dark) in 0.5 M  
196 H<sub>2</sub>SO<sub>4</sub> and the results are illustrated in **Figure 5(a)**. Similarly, LSVs for *chloride oxidation*, i.e.  
197 reaction (1), were recorded for the n-Si/TiO<sub>2</sub>/Ir photoanode – under 1 sun illumination, and the p+-  
198 Si/TiO<sub>2</sub>/Ir anode (in the dark) in a (0.5 M H<sub>2</sub>SO<sub>4</sub> plus 3.5 M NaCl) electrolyte and the results are  
199 illustrated in **Figure 5(b)**. The broken vertical lines highlight the formal redox potentials, E<sup>o</sup>, of the  
200 O<sub>2</sub>/H<sub>2</sub>O (black) and Cl<sup>-</sup>/Cl<sub>2</sub> (red) couples in 0.5 M H<sub>2</sub>SO<sub>4</sub> and (0.5 M H<sub>2</sub>SO<sub>4</sub> plus 3.5 M NaCl)  
201 electrolytes, respectively, calculated, using the Nernst equation, to be: 1.212 and 1.328 V,  
202 respectively.

203 The data associated with each of the LSV's illustrated in **Figure 5** provides a good fit to the Tafel  
204 equation, i.e. <sup>23</sup>

$$205 \quad \eta = a + b \cdot \log(i) \quad (4)$$

206 where, η = overpotential (= applied bias, V<sub>b</sub>, - E<sup>o</sup>), *a* and *b* are constants (units: V) and *i* is the current  
207 density (units: mA cm<sup>-2</sup>). It follows from eqn (4) that the value of the constant '*a*' is the overpotential  
208 necessary to generate a current/photocurrent density of 1 mA cm<sup>-2</sup> and '*b*' is the Tafel slope, which can  
209 provide an insight into the mechanism that underpins the associated electrochemical oxidation. A  
210 summary of the *a* and *b* terms determined by this analysis for the two electrodes in the two different  
211 electrolytic solutions, derived from Tafel plots of the data in **Figure 5**, is given in **Table 1**. The '*a*'

212 values in parenthesis for water oxidation are those reported by Chen et al.<sup>13</sup> for similar electrodes,  
213 although with a thicker Ir layer, i.e. 3 nm rather than the 2 nm used here, and in 1 M H<sub>2</sub>SO<sub>4</sub>.  
214 Reassuringly both studies report a very similar photovoltage, i.e. 0.568 V compared with the value of  
215 0.532 V reported by Chen et al.<sup>13</sup>. As noted by these workers, this photovoltage is similar to that of  
216 the best Si photoelectrochemical solar cells.<sup>24</sup>

217 **Table 1** shows the Tafel slope to be between 70-80mV/decade, with previous works reporting Tafel  
218 slopes in the range of 34-54mV/decade<sup>5,25,26</sup> for iridium oxide catalysts. Slopes around 40mV/decade  
219 are commonly attributed to a Heyrovsky-type rate limiting step,<sup>27</sup> and are associated with  
220 electrochemical desorption being slow.<sup>5</sup> It is worth noting that these previous works study iridium  
221 oxide materials, synthesized either by electrochemical cycling or thermal decomposition<sup>25</sup>. This work  
222 employs an iridium metal catalyst that may not fully oxidize during operation, which may result in  
223 different Tafel slopes for those more reduced regions. This is in agreement with Tilak's work, which  
224 subjected iridium anodes to cathodic current prior to testing and saw higher Tafel slopes (46-  
225 54mV/decade) for a more reduced iridium catalyst.<sup>5</sup> Despite these slightly sub-optimal Tafel slopes,  
226 these ALD-TiO<sub>2</sub> protection layers have been shown to support a wide variety of catalyst materials for  
227 the water oxidation reaction<sup>19,28</sup>, implying the protection layer is robust enough to support further  
228 optimization of the catalyst layer.

229

### 230 *Cl<sub>2</sub> yield and stability*

231 As note earlier, examination of either the CV data in **Figure 4**, or the LSV data in **Figure 5**, reveals a  
232 significant separation (i.e. ca. 0.290 V from data in **Table 1**) between the two photocurrent LSV plots  
233 for the n-Si/TiO<sub>2</sub>/Ir, under 1 sun illumination, in the two different electrolytes, 0.5 M H<sub>2</sub>SO<sub>4</sub> and (0.5  
234 M H<sub>2</sub>SO<sub>4</sub> + 3.5 M NaCl), respectively. A similar separation is found for the p+-Si/TiO<sub>2</sub>/Ir anode (i.e.  
235 0.294 V from data in **Table 1**). This feature suggests that when operated at a modest photocurrent, or  
236 current, (i.e. 1-2 mA) the n-Si/TiO<sub>2</sub>/Ir photoanode, or p+-Si/TiO<sub>2</sub>/Ir anode, should, almost exclusively,  
237 mediate the oxidation of chloride, reaction (1), rather than that of water, reaction (2), so that the yield

238 of chlorine should be very high. In order to test this prediction, the Si/TiO<sub>2</sub>/Ir photoanode (under 1  
239 sun irradiation, polarized at 0.72 V vs Ag/AgCl) and the p<sup>+</sup>-Si/TiO<sub>2</sub>/Ir anode (in dark, polarized at  
240 1.18 V vs Ag/AgCl) were operated in chronoamperometric mode for 1 hour, during which not only  
241 was the current monitored but also any chlorine generated in the electrochemical cell was swept, by a  
242 continual stream of Ar, from the electrolyte to an aqueous trap solution (100 cm<sup>3</sup>), comprising a  
243 mixture of KI (0.36 M), NaOH (0.025 M) and potassium hydrogen phthalate (0.049 M)<sup>29</sup>. Previous  
244 work has demonstrated that the latter solution acts as a very efficient trap for chlorine in a stream of  
245 an inert gas, but not for oxygen. In the trap the Cl<sub>2</sub> reacts with the iodide in the trap solution to form  
246 tri-iodide, the concentration of which can then be assessed spectrophotometrically, given the molar  
247 absorptivity  $\epsilon(\text{I}_3^-) = 26400 \text{ L cm}^{-1} \text{ mol}^{-1}$  at 353 nm.<sup>14</sup>

248 **Figure 6** illustrates the chronoamperograms recorded for the Si/TiO<sub>2</sub>/Ir photoanode and the p<sup>+</sup>-  
249 Si/TiO<sub>2</sub>/Ir anode in an electrolyte of (0.5 M H<sub>2</sub>SO<sub>4</sub> + 3.5 M NaCl). The initial drift downwards in  
250 current does not appear to be due to the loss of electrocatalyst as the same feature was observed in a  
251 repeat experiment using the same, used, electrodes and was also observed when an Ir rod was used as  
252 the anode. Instead, it appears to be due to gas bubble formation on the surface of the electrodes.  
253 From the ratio of the total amount of triiodide trapped ( $3.13 \times 10^{-6}$  moles for the n-Si/TiO<sub>2</sub>/Ir  
254 photoanode) to the total amount of charge passed ( $Q = 0.71 \text{ C}$  for the n-Si/TiO<sub>2</sub>/Ir photoanode)  
255 Faradaic efficiencies for Cl<sub>2</sub> production were determined to be 85% and 92% for the nSi/TiO<sub>2</sub>/Ir  
256 photoanode and the p<sup>+</sup>-Si/TiO<sub>2</sub>/Ir anode, respectively. Similar yields were determined using an Ir rod  
257 as the anode and also a dimensionally stable anode, comprising a film of RuO<sub>2</sub>/TiO<sub>2</sub> on a Ti foil<sup>30</sup>,  
258 and the slightly less than 100% Faradaic efficiencies for Cl<sub>2</sub> production for all these electrodes was  
259 attributed to a small degree of reaction of the very aggressively oxidising chlorine with the  
260 components of the system as it was swept from the electrochemical cell to the trap solution.

261 Chlorine is a very reactive oxidising agent, thus any protective coating has to be sufficiently robust  
262 *chemically* to withstand the highly corrosive action of chlorine in a highly acidic environment.  
263 Without this TiO<sub>2</sub> coating, even with an Ir catalyst layer, none of the p<sup>+</sup>-Si and n-Si anodes are stable  
264 and able to effect the oxidation of either water or chloride. In order to probe the stability of the TiO<sub>2</sub>

265 protective coating and the overall photostability of the photoanode, a chronopotentiogram was  
266 recorded, with the current set at  $1 \text{ mA cm}^{-2}$ , for the Si/TiO<sub>2</sub>/Ir photoanode (irradiated with a UV 455  
267 nm LED;  $6.5 \text{ mW cm}^{-2}$ ) over a period of ca 6 days and the results are illustrated in **Figure 7**.

268 The short disruption in the current –time plot at 3 d, see **Figure 7**, was due to Cl<sub>2</sub> bubble formation,  
269 which – once cleared – allowed the photoelectrode to function as before. The %Cl<sub>2</sub> yield was  
270 measured for the first and last hour of this run and found to be in both cases ca. 85% as in **Figure 6**.

271 The results illustrated in **Figure 7** indicate that the n-Si/TiO<sub>2</sub>/Ir photoanode is stable over a 6-day  
272 period when used to photo-electrochemically oxidized chloride to chlorine under acidic conditions.

273 Films as-deposited are conformal, metallic iridium films, and remain unbroken after stability testing.  
274 X-ray Photoelectron Spectroscopy confirms the iridium oxidizes during stability measurements, but  
275 retains both oxide and metallic components. (see **Figures S2-4**) Scanning Auger Electron  
276 Microscopy confirms the iridium film remains intact, with only slight carbon contamination. (**Figure**  
277 **S4**)

### 278 *Efficiency*

279 Finally, the n-Si/TiO<sub>2</sub>/Ir photoanode was used in a 2-electrode format, using a wound Pt wire (surface  
280 area =  $2.5 \text{ cm}^2$ ) as the counter electrode and the photocurrents,  $i$ , measured under 1 sun illumination as  
281 a function of applied bias,  $V_b$  (in volts), in the following electrolytes: 0.5 M H<sub>2</sub>SO<sub>4</sub> (water oxidation)  
282 and (0.5 M H<sub>2</sub>SO<sub>4</sub> plus 3.5 M NaCl) (chloride oxidation). These data were then used to calculate the  
283 applied bias photon-to-current efficiency (ABPE) for the photocleavage of water and the  
284 photoelectrolysis of the acidified brine by the n-Si/TiO<sub>2</sub>/Ir photoanode under 1 sun illumination, based  
285 on the following expression:

$$286 \quad \text{ABPE} = i(\text{mA cm}^{-2}) \times (E_{\text{ref}} - V_b) / P_{\text{total}} (\text{mW cm}^{-2}) \quad (5)$$

287 where,  $E_{\text{ref}} = 1.212 \text{ V}$  in 0.5 M H<sub>2</sub>SO<sub>4</sub> (for water oxidation) and  $1.328 \text{ V}$  in (0.5 M H<sub>2</sub>SO<sub>4</sub> plus 3.5 M  
288 NaCl) (for chloride oxidation) and  $P_{\text{total}} = \text{incident illumination power density} = 100 \text{ mW cm}^{-2}$ ; note:  
289 this equation assumes 100% Faradaic efficiency in the production of O<sub>2</sub> or Cl<sub>2</sub>.

290 The plots of ABPE vs  $V_b$  are illustrated in **Figure 8** and reveal maximum values for water splitting  
291 and acidified brine photoelectrolysis of 0.05 % and 1.42 %, respectively. The 28 times increase in  
292 efficiency for the photo-oxidation of the brine, compared to that of water in acid solution is primarily  
293 due to the fact that the overpotential for the former reaction is much lower than that for the latter, see  
294 **Table 1**, so that a greater fraction of the photovoltage, ca. 560 mV is utilized for fuel ( $H_2$ ) and  
295 disinfectant ( $Cl_2$ ) production. The ABPE value of 1.42 % compares very well with that of 0.6%  
296 reported by Kim et al.<sup>31</sup> for their record-breaking single crystal, worm-like hematite photoanodes for  
297 water oxidation, although, in the latter case, the value of 0.6% is flattered by the use of a 3-electrode  
298 cell, which excludes any loss in efficiency due to the counter electrode reaction, as is found for many  
299 reported ABPE and Solar to Hydrogen Efficiency (STH) values.<sup>32</sup> As noted earlier, ultimately the  
300 photoanode will be paired with an appropriate photocathode in a tandem cell, or be made part of a  
301 photovoltaic triple junction, which will reduce significantly the value for  $V_b$  and so improve markedly  
302 the value of ABPE. However, as it stands this is the first use of a low bandgap semiconductor  
303 photoanode to photoelectrolyze (acidified) brine so as to generate a fuel ( $H_2$ ) and a disinfectant ( $Cl_2$ )  
304 with an efficiency superior to that of leading reported photoanodes used to photodissociate water.<sup>31</sup>

#### 305 **IV. Conclusion**

306 An n-type silicon photoanode, utilizing a 2 nm thin film iridium catalyst protected by a 1.7 nm  
307 thickness coating of atomic layer deposited amorphous  $TiO_2$ , is able to effect the photo-oxidation of  
308 water to  $O_2$  and of chloride to  $Cl_2$ , with an incident photon-to-current efficiency that increases with  
309 increasing bias voltage, eventually reaching ca. 100% efficiency if light loss due to Ir film absorption  
310 is taken into consideration. In 0.5 M  $H_2SO_4$  acid, the photo-oxidation of water occurs at potentials  
311 that are ca. 290 mV greater than that for chloride oxidation (0.5 M  $H_2SO_4$  plus 3.5 M NaCl), which  
312 allows the n-Si/ $TiO_2$ /Ir photoanode (1 sun illumination) and dark p<sup>+</sup>-Si/ $TiO_2$ /Ir anode to generate  $Cl_2$   
313 with a high (>85 %) yield. Applied bias photon-to-current efficiencies of 0.05% and 1.42 % were  
314 determined for the n-Si/ $TiO_2$ /Ir photoanode for water and chloride oxidation respectively. The latter  
315 value is particularly encouraging, especially given the potential for improvement when the n-  
316 Si/ $TiO_2$ /Ir photoanode is coupled to an appropriate photocathode in a tandem cell, or used in a triple

317 junction photovoltaic. This initial study illustrates the effectiveness of layered ALD-TiO<sub>2</sub> and Ir thin  
318 film coatings in simultaneously protecting silicon photoanodes from corrosion and achieving low  
319 overpotentials and large photovoltages to generate both a fuel but a disinfectant and a water  
320 disinfectant in a photoelectrochemical device.  
321

322 **References**

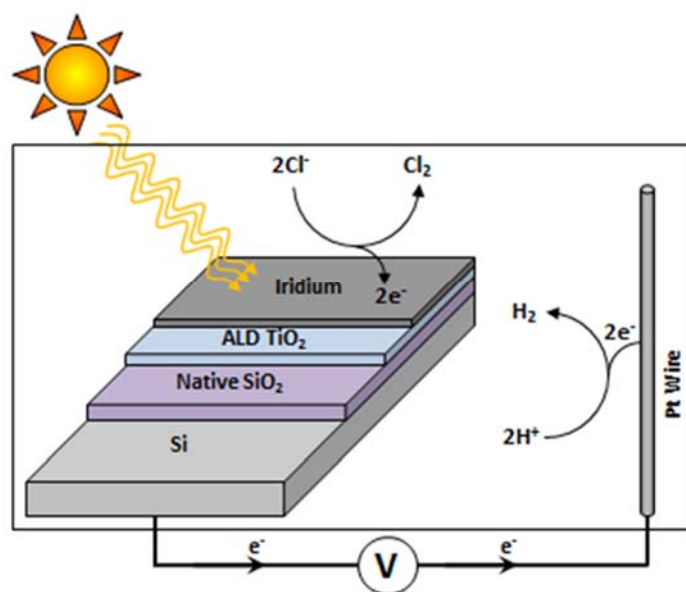
- 323 1. Lewis, N. S. & Nocera, D. G. Powering the planet: Chemical challenges in solar  
324 energy utilization. *Proc. Natl. Acad. Sci.* **103**, 15729–15735 (2006).
- 325 2. Walter, M. G. *et al.* Solar Water Splitting Cells. *Chem. Rev. (Washington, DC, United*  
326 *States)* **110**, 6446–6473 (2010).
- 327 3. Rahim, S. Energy from a Water Bottle. *Scientific American* (2010). at  
328 <<https://www.scientificamerican.com/article/energy-from-a-water-bottle/>>
- 329 4. Reece, S. Y. *et al.* Wireless Solar Water Splitting Using Silicon-Based  
330 Semiconductors and Earth-Abundant Catalysts. *Science (80-. )*. **334**, 645–648 (2011).
- 331 5. Tilak, B. V. Kinetics of Chlorine Evolution—A Comparative Study. *J. Electrochem.*  
332 *Soc.* **126**, 1343 (1979).
- 333 6. EuroChlor. What is chlorine used for? (2017). at <[http://www.eurochlor.org/the-](http://www.eurochlor.org/the-chlorine-universe/what-is-chlorine-used-for.aspx)  
334 [chlorine-universe/what-is-chlorine-used-for.aspx](http://www.eurochlor.org/the-chlorine-universe/what-is-chlorine-used-for.aspx)>
- 335 7. Sodis. Sodis: Safe Drinking Water For All. (2016). at  
336 <[http://www.sodis.ch/index\\_EN](http://www.sodis.ch/index_EN)>
- 337 8. Beer, H. B. The Invention and Industrial Development of Metal Anodes. *J.*  
338 *Electrochem. Soc.* **127**, 303C (1980).
- 339 9. Hu, S. *et al.* Thin-Film Materials for the Protection of Semiconducting Photoelectrodes  
340 in Solar-Fuels Generators. *J. Phys. Chem. C* 150928141004000 (2015).  
341 doi:10.1021/acs.jpcc.5b05976
- 342 10. Aromaa, J. & Forsén, O. Evaluation of the electrochemical activity of a Ti-RuO<sub>2</sub>-TiO<sub>2</sub>  
343 permanent anode. *Electrochim. Acta* **51**, 6104–6110 (2006).
- 344 11. Morita, M., Iwakura, C. & Tamura, H. The anodic characteristics of modified Mn  
345 oxide electrode: Ti/RuO<sub>x</sub>/MnO<sub>x</sub>. *Electrochim. Acta* **23**, 331–335 (1978).
- 346 12. Duby, P. The history of progress in dimensionally stable anodes. *JOM* **45**, 41–43



- 347 (1993).
- 348 13. Chen, Y. W. *et al.* Atomic layer-deposited tunnel oxide stabilizes silicon photoanodes  
349 for water oxidation. *Nat. Mater.* **10**, 539–544 (2011).
- 350 14. Mills, A. & Cook, A. Analysis of chlorine - oxygen gas mixtures. *Analyst* **112**, 1289–  
351 1291 (1987).
- 352 15. Meng, H., Fan, K., Low, J. & Yu, J. Electrochemically reduced graphene oxide on  
353 silicon nanowire arrays for enhanced photoelectrochemical hydrogen evolution. *Dalt.*  
354 *Trans.* **45**, 13717–13725 (2016).
- 355 16. Hu, S. *et al.* Amorphous TiO<sub>2</sub> coatings stabilize Si, GaAs, and GaP photoanodes for  
356 efficient water oxidation. *Science* **344**, 1005–9 (2014).
- 357 17. Bae, D. *et al.* Back-Illuminated Si-Based Photoanode with Nickel Cobalt Oxide  
358 Catalytic Protection Layer. *ChemElectroChem* **3**, 1517 (2016).
- 359 18. Li, C. *et al.* Efficient photoelectrochemical water oxidation enabled by an amorphous  
360 metal oxide-catalyzed graphene/silicon heterojunction photoanode. *Sustain. Energy*  
361 *Fuels* 663–672 (2018). doi:10.1039/C7SE00504K
- 362 19. Scheuermann, A. G., Prange, J. D., Gunji, M., Chidsey, C. E. D. & McIntyre, P. C.  
363 Effects of catalyst material and atomic layer deposited TiO<sub>2</sub> oxide thickness on the  
364 water oxidation performance of metal–insulator–silicon anodes. *Energy Environ. Sci.*  
365 **6**, 2487 (2013).
- 366 20. Campet, G., Manaud, J. P., Puprichitkun, C., Sun, Z. W. & Salvador, P. Protection of  
367 photoanodes against photo-corrosion by surface deposition of oxide films: criteria for  
368 choosing the protective coating. *Act. Passiv. Electron. Components* **13**, 175–189  
369 (1989).
- 370 21. Batzill, M., Katsiev, K., Gaspar, D. J. & Diebold, U. Variations of the local electronic  
371 surface properties of TiO<sub>2</sub> (110) induced by intrinsic and extrinsic defects. *Phys. Rev.*

- 372 *B* **66**, 235401 (2002).
- 373 22. Papageorgiou, A. C. *et al.* Electron traps and their effect on the surface chemistry of  
374 TiO<sub>2</sub>(110). *Proc. Natl. Acad. Sci.* **107**, 2391–2396 (2010).
- 375 23. Bagotsky, V. S. *Fundamentals of Electrochemistry*. (Wiley-Interscience, 2006).
- 376 24. Switzer, J. A. The n-Silicon/Thallium(III) Oxide Heterojunction Photoelectrochemical  
377 Solar Cell. *J. Electrochem. Soc.* **133**, 722 (1986).
- 378 25. Consonni, V., Trasatti, S., Pollak, F. & O’Grady, W. E. Mechanism of chlorine  
379 evolution on oxide anodes study of pH effects. *J. Electroanal. Chem.* **228**, 393–406  
380 (1987).
- 381 26. Mozota, J. Modification of Apparent Electrocatalysis for Anodic Chlorine Evolution  
382 on Electrochemically Conditioned Oxide Films at Iridium Anodes. *J. Electrochem.*  
383 *Soc.* **128**, 2142 (1981).
- 384 27. Shinagawa, T., Garcia-Esparza, A. T. & Takanabe, K. Insight on Tafel slopes from a  
385 microkinetic analysis of aqueous electrocatalysis for energy conversion. *Sci. Rep.* **5**, 1–  
386 21 (2015).
- 387 28. McDowell, M. T. *et al.* The Influence of Structure and Processing on the Behavior of  
388 TiO<sub>2</sub> Protective Layers for Stabilization of n-Si/TiO<sub>2</sub>/Ni Photoanodes for Water  
389 Oxidation. *ACS Appl. Mater. Interfaces* (2015). doi:10.1021/acsami.5b00379
- 390 29. Hernández-Pagán, E. A. *et al.* Resistance and polarization losses in aqueous buffer-  
391 membrane electrolytes for water-splitting photoelectrochemical cells. *Energy Environ.*  
392 *Sci.* **5**, 7582–7589 (2012).
- 393 30. O’Brien, T. F., Bommaraju, T. V & Hine, F. in *Handbook of Chlor-Alkali Technology:*  
394 *Volume I: Fundamentals* (Springer USA, 2005). doi:10.1007/0-306-48624-5\_5
- 395 31. Kim, J. Y. *et al.* Single-crystalline, wormlike hematite photoanodes for efficient solar  
396 water splitting. *Sci. Rep.* **3**, 1–8 (2013).

- 397 32. Chen, Z., Dinh, H. & Miller, E. *Photoelectrochemical Water Splitting: Standards,*  
398 *Experimental Methods, and Protocols.* (Springer, 2013).  
399  
400

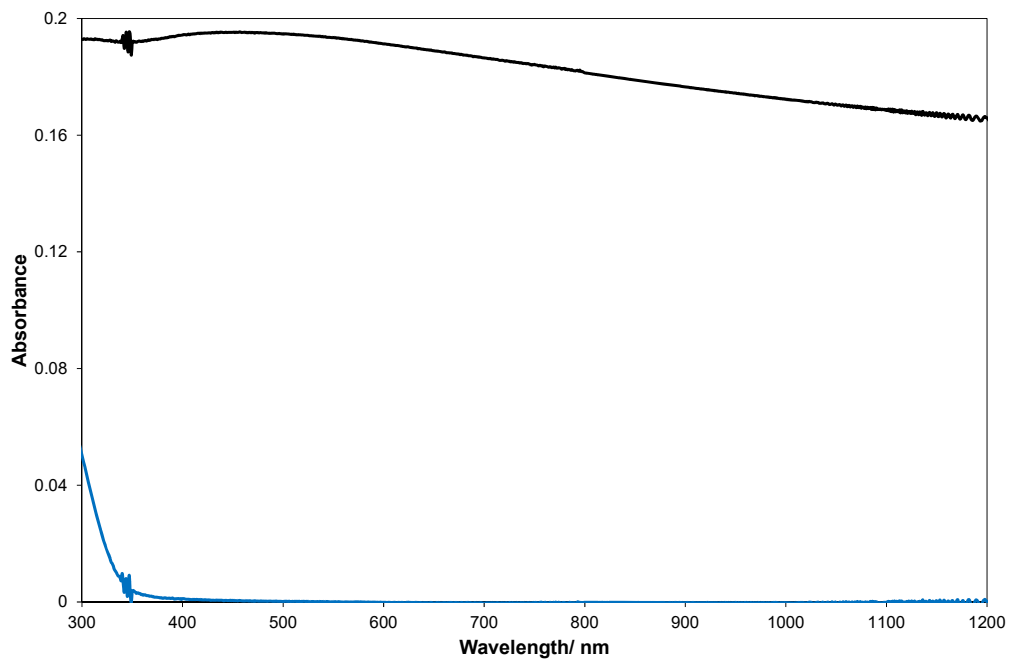


401

402 **Figure 1:** Schematic illustration of the n-Si/TiO<sub>2</sub>/Ir photoanode used to photo-oxidize chloride (3.5 M

403 NaCl) to chlorine in acid (0.5 M H<sub>2</sub>SO<sub>4</sub>)

404

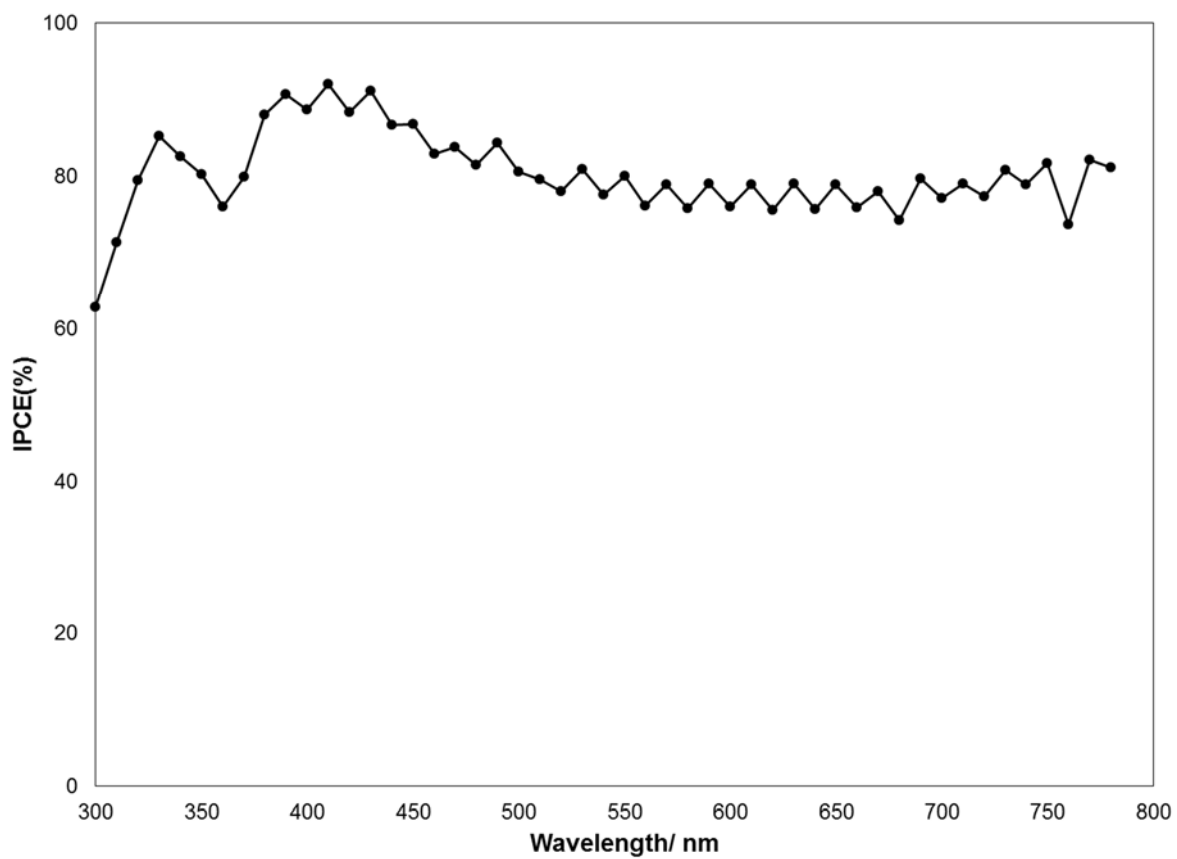


405

406 **Figure 2:** UV/Vis/NIR spectra of the following films on quartz: (i) 2 nm of evaporated Ir (black line)

407 and (ii) 1.7 nm of ALD-deposited amorphous TiO<sub>2</sub> (blue line).

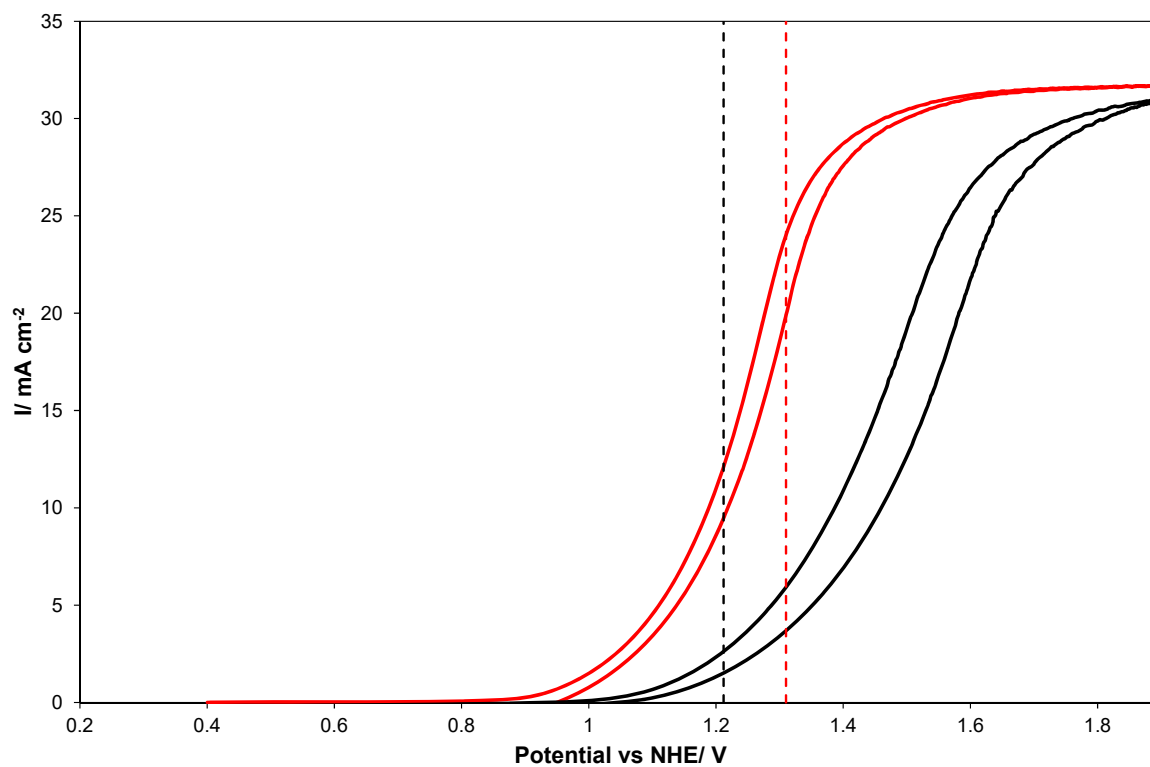
408



409

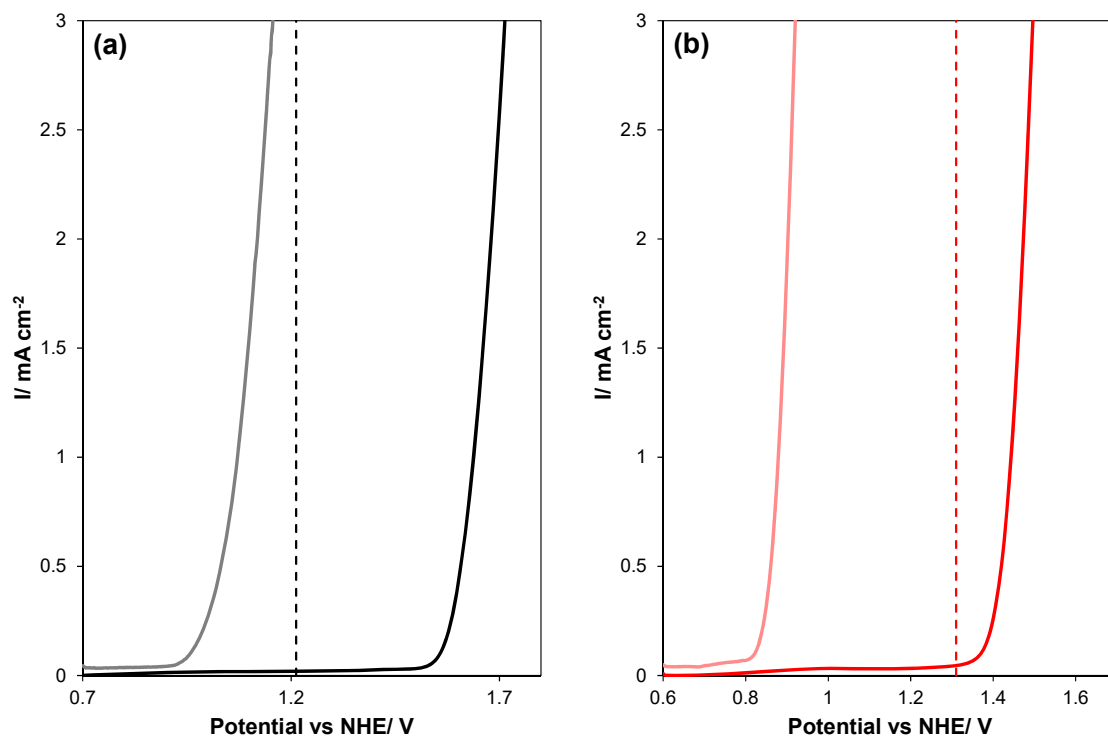
410 **Figure 3:** IPCE spectrum of the n-Si / 2 nm TiO<sub>2</sub> / 2nm Ir anode at 1.8V vs NHE and a 0.8cm<sup>2</sup> active  
411 area. Electrolyte was 0.5 M H<sub>2</sub>SO<sub>4</sub> + 3.5 M NaCl.

412



413

414 **Figure 4:** CVs for the n-Si/TiO<sub>2</sub>/Ir photoanode under 1 sun irradiation, sweep rate: 100 mV s<sup>-1</sup>  
 415 recorded in 0.5 M H<sub>2</sub>SO<sub>4</sub> (black line) or 0.5 M H<sub>2</sub>SO<sub>4</sub> plus 3.5 M NaCl (red line) under 1 sun  
 416 irradiation, i.e. 100 mW cm<sup>-2</sup>. The broken vertical lines represent the thermodynamic potentials for  
 417 reaction (1) (broken red line) and reaction (2) (broken black line).



418

419 **Figure 5:** LSV curves for (from left to right): a p+-Si/TiO<sub>2</sub>/Ir anode (in the dark) and an n-Si/TiO<sub>2</sub>/Ir,  
 420 under 1 sun irradiation, in (a) 0.5 M H<sub>2</sub>SO<sub>4</sub> (black lines) and (b) (0.5 M H<sub>2</sub>SO<sub>4</sub> + 3.5 M NaCl), (red  
 421 lines) respectively. The broken vertical lines in (a) and (b) represent the thermodynamic potentials for  
 422 reaction (1) (red line) and reaction (2) (black line), respectively.



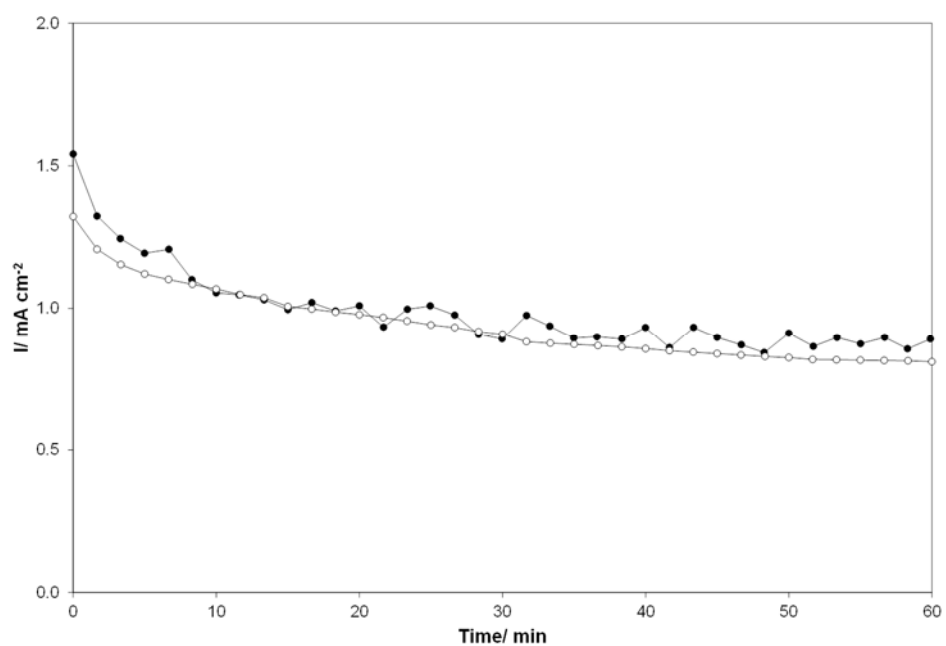
423 **Table 1:** Results of Tafel plot analysis of LSVs for the Si/TiO<sub>2</sub>/Ir photoanode and p+-Si/TiO<sub>2</sub>/Ir  
 424 anode

Anode	$a/V$	$b/V$	$V_{\text{photo}}\ddagger/V$
<b>Water oxidation (0.5 M H<sub>2</sub>SO<sub>4</sub>)</b>			
p+-Si/TiO <sub>2</sub> /Ir	0.428 (0.332) $\ddagger$	0.122	0.568 (0.532)
n-Si/TiO <sub>2</sub> /Ir*	-0.140 (-0.200)	0.144	
<b>Chloride oxidation (0.5 M H<sub>2</sub>SO<sub>4</sub> + 3.5 M NaCl)</b>			
p+-Si/TiO <sub>2</sub> /Ir	0.134	0.089	0.564
n-Si/TiO <sub>2</sub> /Ir*	-0.430	0.069	

425 \* 1 sun irradiation; 1100 mW cm<sup>-2</sup>

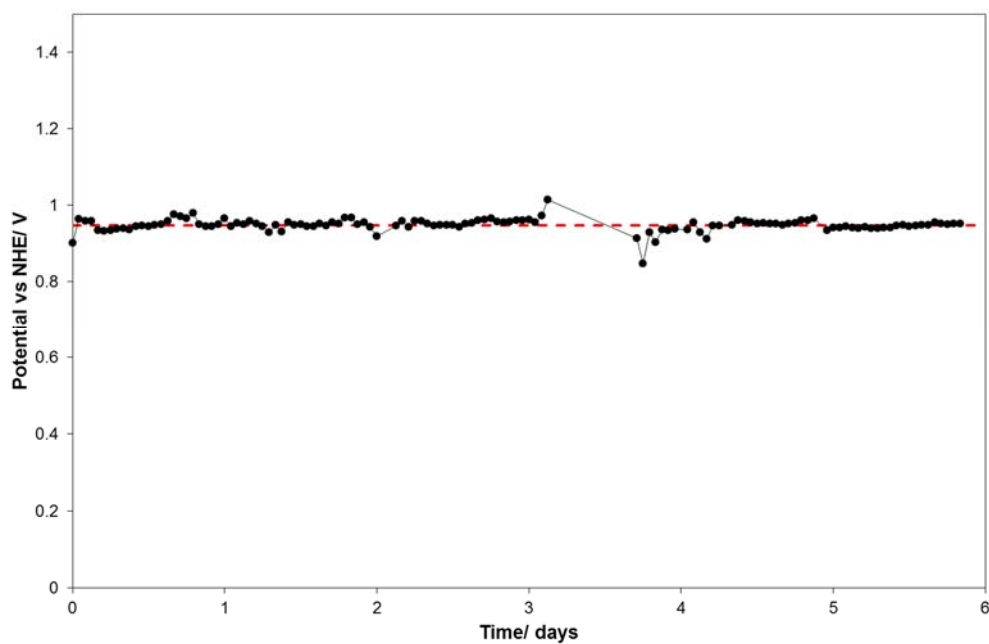
426 †:  $V_{\text{photo}} = \text{photovoltage} = a(\text{n-Si/TiO}_2/\text{Ir}^*) - a(\text{p+-Si/TiO}_2/\text{Ir})$

427 ‡: Values reported by Chen et al in 1 M H<sub>2</sub>SO<sub>4</sub>



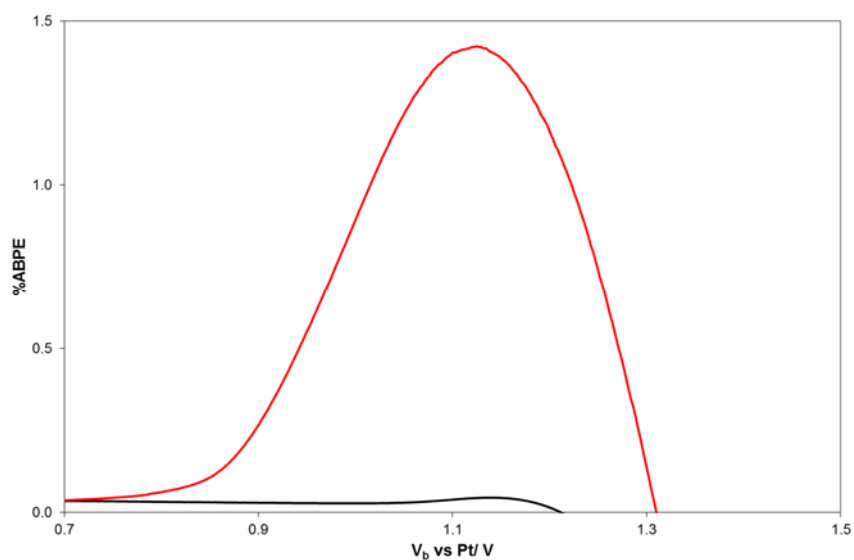
428

429 **Figure 6:** Chronoamperograms recorded using the electrochemical cell illustrated in figure S1 and  
 430 either: (i) a Si/TiO<sub>2</sub>/Ir photoanode, ●, (under 1 sun irradiation, polarized at 0.72 V vs Ag/AgCl), or  
 431 (ii) a p<sup>+</sup>-Si/TiO<sub>2</sub>/Ir anode, ○ (in dark, polarized at 1.18 V vs Ag/AgCl) using a electrolyte of: (0.5 M  
 432 H<sub>2</sub>SO<sub>4</sub> + 3.5 M NaCl).



433

434 **Figure 7:** Six-day chronopotentiometry runs, at  $1 \text{ mA cm}^{-2}$ , recorded using the electrochemical cell  
435 illustrated in **Figure S1** with an n-Si/TiO<sub>2</sub>/Ir photoanode, ●, (under 455 nm LED irradiation,  $6.5 \text{ mW}$   
436  $\text{cm}^{-2}$ ), with an electrolyte of (0.5 M H<sub>2</sub>SO<sub>4</sub> + 3.5 M NaCl) and the current set at  $1 \text{ mA cm}^{-2}$ . The  
437 average applied potential was 0.95V (broken red line)



438

439 **Figure 8:** ABPE vs bias potential with respect to the Pt counter electrode,  $V_b$  plot for the n-Si/TiO<sub>2</sub>/Ir  
440 photoanode under 1 sun illumination in 0.5 M H<sub>2</sub>SO<sub>4</sub> (for water oxidation – black line) and in 0.5 M  
441 H<sub>2</sub>SO<sub>4</sub> plus 3.5 M NaCl (for chloride oxidation – red line)